**Synapsin knockdown is associated with decreased neurite outgrowth, functional synaptogenesis impairment, and fast high-frequency neurotransmitter release**

**Title**

Synapsin knock-down is associated with decreased neurite outgrowth, functional synaptogenesis impairment and fast high frequency neurotransmitter release.

**Authors**

Brenes Oscar [1,2]

Giachello Carlo Natale Giuseppe [3]

Corradi Anna Margherita [4]

Ghirardi Mirella [1,5]

Montarolo Pier Giorgio [1,5]

**Institutional Affiliation**

1 Department of Neuroscience, Section of Physiology, University of Turin, Turin, Italy.

2 Department of Physiology, School of Medicine, University of Costa Rica, San José, Costa Rica.

3 Faculty of Life Sciences, University of Manchester, Manchester, UK.

4 Department of Experimental Medicine, University of Genova, Genova, Italy

5 National Institute of Neuroscience, Turin, Italy.

**Abbreviated title**

Synapsin knock-down induced alterations.

**Keywords**

Synapsins, Invertebrates, Synaptic Transmission, Synapses, Neurites,

NCBI Taxonomic ID: 6535, RRID: nif-0000-00313, RRID: nif-0000-30467, RRID: AB_11181145, RRID: rid_000085, RRID: rid_000081.

**Corresponding author**

Oscar Brenes. Department of Physiology, School of Medicine, University of Costa Rica, 2060, San José, Costa Rica. Tel: +506 2511 4391; Fax: +506 2511 4482;

Email addresses: oscar.brenes_g@ucr.ac.cr, oscar.brenesgarcia@edu.unito.it

**Grant information**

This work was supported by Grants from Italian Ministry of the University and Research (PRIN 2009 grants to PGM) and Compagnia di San Paolo (to PGM and MG).

**Abstract**

Synapsins are an evolutionarily-conserved family of synaptic vesicle-associated proteins, related to fine-tuning of synaptic transmission. Studies in mammals have partially clarified the different roles of synapsins, however the presence of different genes and isoforms and the development of compensatory mechanisms hinder accurate data interpretation. Here, we used a simple *in vitro* monosynaptic *Helix*-neurons connection, reproducing an *in vivo* physiological connection, as a reliable experimental model, in order to investigate the effects of synapsin knock-down. Cells overexpressing an antisense construct against *Helix* synapsin showed a time-dependent decrease of synapsin immunostaining, confirming protein loss. At the morphological level, synapsin-silenced cells showed a reduction in neurite linear outgrowth and branching, and in the size and number of synaptic varicosities. Functionally, synapsin-silenced cells presented a reduced ability to form synaptic connections; however functional chemical synapses showed similar basal excitatory postsynaptic potentials and similar short-term plasticity paradigms. In addition, synapsin-silenced cells presented faster neurotransmitter release, and decreased postsynaptic response toward the end of long tetanic presynaptic stimulations, probably related to an impairment of the synaptic vesicles trafficking due to a different vesicle handling, with an increased readily releasable pool and a compromised reserve pool.

**Significance Statement**

Synapsins are a family of presynaptic proteins associated with several cellular processes, whose mutations have been associated with different pathologies. The characterization of the specific role of synapsins in synapse establishment and function in simple models will help to understand the genesis of these pathologies in more complex organisms. Using a monosynaptic model our results highlight the relevant role of synapsins promoting neurite-outgrowth and formation of functional synapses, and regulating the fine-tuning of neurotransmitter release, modulating the size of the readily releasable pool of synaptic vesicles and the capacity to respond to high-frequency stimulation.

## Introduction

The transmission of information in the nervous system depends on proper formation and functioning of a complex array of neuronal circuits, processes that requires a fine regulation of complex mechanisms (Washbourne et al., 2004). Deficiencies in processes like neurite-outgrowth, synapse formation or neurotransmitter release would have inevitable consequences on nervous system functioning, leading to development of behavioral and/or cognitive diseases.

The synapsins (Syns) are an evolutionarily-conserved family of presynaptic vesicle-associated phospho-proteins that play a major role in the fine-tuning of synapse function. Furthermore, Syns mutations in humans have been associated to different pathologies (Cesca et al., 2010; Garcia et al., 2004; Fassio et al., 2011; Greco et al., 2013; Corradi et al., 2014).

Depletion of SynI, II or III results in inhibition of formation and maintenance of synapses and aberrant neuritic outgrowth or impaired axonal differentiation (Ferreira et al., 1994, 1995, 1998, 2000). However, some aspects regarding their functional role in neuronal development are still controversial, since it has been reported that SynI/II double deletion largely decreased the developmental deleterious effects of individual deletions (Ferreira et al., 1998) and knocking out all three Syn genes (TKO) resulted in cells presenting milder development impairments and no significant alterations in gross neuronal development (Gitler et al., 2004b; Cesca et al., 2010; Valtorta et al., 2011).

It is also well accepted that Syns influence synapse formation and acts in the modulation of synaptic vesicle (SV) pools (Gaffield and Betz, 2007; Valtorta et al., 2011; Orenbuch et al., 2012). However, the exact function is still unclear since there are conflicting reports about the Readily Releasable Pool (RRP) size (Gitler et al., 2004b; Kile, 2010; Farisello et al., 2013), the total number of SV, and the amplitude of the excitatory postsynaptic currents (Feng et al.,

2002; Gitler et al., 2004b; Chiappalone et al., 2009; Farisello et al., 2013; Medrihan et al., 2013) in TKO with respect to wild-type (WT) mice.

The discrepancies among single, double and triple knock-out models could reflect the development of compensatory mechanisms in mice lacking two or more Syns, hindering accurate data interpretation (Cesca et al., 2010). The lack of conditional TKO models, which could prevent developmental compensation, hampers the testing of this possibility in mammalian models. In addition, the presence of different genes and isoforms in mammalian Syns with overlapping functions interferes with their clear characterization. For these reasons, we decided to use an *in vitro* monosynaptic *Helix*-neurons connection as a model to study Syn knock-down.

The land snail *Helix* provides several advantages since specific identifiable neurons can be isolated and reliable connections can be formed *in vitro*, culturing physiological synapses that recapitulate *in vivo* features (Ghirardi et al., 1996; Fiumara et al., 2001, 2005) thereby avoiding unspecific effects due to surrounding tissue or random connections. This model has been used in several studies addressing the effects of Syn phosphorylation on synapse function (Ghirardi et al., 1996; Fiumara et al., 2001, 2004, 2007; Giachello et al., 2010). *Helix* neurons provide a convenient genetic organization (Fiumara et al., 2007), a single Syn gene that can be blocked by antisenseRNA (asRNA). And also offer amenability to experimental manipulations such as plasmid intra-nuclear microinjection, allowing the constitutive expression of asRNAs in cells that can be coupled to their physiological target, permitting the silencing of Syn in specific monosynaptic circuits in order to study synapse properties.

## Materials and Methods

### Materials

All chemicals and reagents used in this study were purchased from Sigma (Milan, Italy), unless stated otherwise.

### Animals

Juvenile specimens of *Helix aspersa* land snails (NCBI Taxonomic ID: 6535) were provided by local breeders and maintained inactive at a temperature of 6°C. Before experimental procedures, snails were kept in an active state for at least 16 hr in a climate chamber, regulating temperature and humidity (20°C and 70% relative humidity). During the activity period, snails were fed with lettuce and water *ad libitum*. During surgical procedures, the snails were always anesthetized and efforts were made to minimize the number and suffering of animals used, in accordance with Directive 2010/63/EU of the European Parliament and of the Council of 22 September 2010 on the protection of animals used for scientific purposes.

### Cell Culture

Cell cultures were performed as previously described (Ghirardi et al., 1996). Briefly, snails were anesthetized by the injection of isotonic $MgCl_2$ in the foot. Cerebral and buccal ganglia were surgically isolated and incubated for enzymatic digestion in protease type XIV in isotonic L15 medium (0.3 U/ml) at 34°C for 3-3.5 hr. After digestion, the ganglia were washed two times in L15 medium and C1 and B2 neurons were individually isolated, identified by their position in the ganglia and their size. In experiments with cells plated with their axonal stumps, cells were gently isolated with the initial segment of their original axons still attached to somata and immediately plated on dishes pretreated with poly-L-lysine and *Aplysia* hemolymph. In experiments with axon-reabsorbed somata (soma-configuration) neurons were isolated and transferred to dishes pretreated with 5% bovine serum albumin (BSA) to prevent cell-substrate adhesion, as previously described (Fiumara et al., 2005). After

24 hr floating neurons retracted their processes, obtaining spherical somata. Then, floating somata were gently manipulated according to the specific experimental protocols.

**Plasmid generation and intra-nuclear microinjection**

The plasmid $pNEX_3$ containing EGFP sequence (pNEX-EGFP) was used as a control. Standard recombinant DNA techniques were used to insert the DNA sequence complementary to the 3' third of mRNA of *Helix* synapsin (helSyn) (a fragment of 544 bp) in the $pNEX_3$ plasmid, depleted of EGFP (pNEX-helSynAS). Control cells were intra-nuclear microinjected with the pNEX-EGFP alone, whereas knocked down cells (helSynKD cells) were injected with both pNEX-helSynAS and pNEX-EGFP.

Intra-nuclear microinjection was done with a glass electrode, with the tip filled with a solution containing the plasmids (1 μg/ml each), KCl (0.2 M) and Fast Green solution 0.2 % (p/v), and the cell was loaded using short pressure pulses (10-20 pulses, 2-10 psi) delivered through a pneumatic picopump (PV820, WPI, Sarasota, FL) connected to the electrode holder. The injection procedure was monitored under visual and electrophysiological control and stopped when the nucleus was uniformly colored.

**Measurement of neurite length and branching**

To measure neurite length, bright field images of cultures were acquired using the software Image Pro Plus (Mediacybernetics, Bethesda, MD; RRID: nif-0000-00313) and a Monochrome Evolution QE camera (Mediacybernetics, Bethesda, MD) at 24, 48, 72 and 96 hr after plating. The measurement of neurite length of cells plated with the initial segment of their original axons was performed on axonal extension originating from the tip of the axonal stump. In soma-configuration experiments, the measurement was done on neurites originated from the soma. At least 30 neurites per cell were measured using the freely available software ImageJ 1.44 (NIH, Bethesda, MD; RRID: nif-0000-30467), and their linear elongation was followed in time. The quantification of total amount of neurite field was done as previously

described (Ghirardi et al., 1996). Briefly, concentric rings (at 25 μm intervals) with their center localized in the center of the soma were drawn and the number of intersections with neurites were counted as a general indication of the neurite branching. When necessary brightness and contrast was adjusted in the entire image.

**Immunocytochemistry**

Cultures were washed three times (10 min each) in *Helix* saline solution (NaCl 0.6 %) at room temperature (RT) and then fixed with 4% paraformaldehyde in 0.1 M phosphate-buffered saline (PBS; 45 min, at RT). Afterwards cultures were rinsed in PBS 0.01 M and treated with blocking solution (5% bovine serum albumin and 0.25% saponin in PBS 0.01 M) for 1 hr at RT. The cultures were then incubated overnight at 4°C with a rabbit anti-helSyn custom antibody (1:500 dilution, Table I) in blocking solution. After rinsing with 0.25% saponin in PBS 0.01 M, the cultures were incubated in blocking solution with an Alexa-conjugated anti-rabbit IgG (1:500 dilution; Life Technologies Cat# A10040, RRID: AB_11181145) secondary antibody and after 45 min at RT were washed 3 times in PBS 0.01 M. Finally, cultures were kept in 0.1 M PBS and cell images were captured with a Monochrome Evolution QE camera (Mediacybernetics, Bethesda, MD) using an Eclipse TE200 inverted microscope (Nikon Instruments, Tokyo, Japan) equipped with epifluorescence optics.

**Antibody Characterization**

Table I shows the information of the antibody against helSyn used in this study. The helSyn polyclonal antibody was manufactured by Inbios International Inc. (WA, USA). OVA-conjugated peptide was used for the immunization of a rabbit and the resultant affinity purified polyclonal antibody Ab-105 was tested against free synthetic peptide by ELISA test. Specificity of the custom antibody was tested on Western blot over *Helix* ganglia lysate. The total level of helSyn (phosphorylated or non-phosphorylated) was revealed as a doublet with a molecular mass of approximately 28 kDa.

**helSyn quantification**

Quantitative analysis of fluorescence was performed on areas of 50x50 μm, with an almost complete coverage of the neurite field. To quantify the presence of helSyn in cell varicosities a radiometric imaging analysis, defined as Targeting Factor (TF), was performed as previously described (Gitler et al., 2004a). Briefly, cells were co-injected with the asRNA generating plasmid (pNEX-helSynAS) and pNEX-EGFP. Fluorescence intensity of EGFP and Alexa-conjugated secondary antibody were measured independently (Fig. 1). Using the Line Profile tool of Image Pro Plus we drew a line across the varicosities and the proximal neurites, obtaining a plot of the pixel intensity values for each wavelength, corrected for the measured local background values. The peak of fluorescence of the line profile represents varicosity intensity while tails represent the proximal neurites. The ratio of intensities of fluorescence produced by the Alexa-conjugated antibody against helSyn antibody (SynAb) was corrected for variations in cell volume using the ratio of fluorescence of the free diffusion dye EGFP according to equation 1. Thus, a decrease in the value of the targeting factor represents a reduction in helSyn protein.

$$\text{Targeting Factor} = \frac{\text{Varicosity}_{\text{SynAb}}/\text{Neurite}_{\text{SynAb}}}{\text{Varicosity}_{\text{EGFP}}/\text{Neurite}_{\text{EGFP}}} - 1 \qquad \text{EQN 1}$$

**Varicosity analysis**

A roughly spherical structure with an area between 2 and 25 $\mu m^2$ was considered as a varicosity. Cell varicosities were counted manually using micrographs of the whole neuritic field of each cell (10X magnification). Varicosity areas were digitally measured on micrographs (60X magnification) with an almost complete coverage of the neurite field. When necessary brightness and contrast was adjusted in the entire micrograph.

**Electrophysiological recordings**

Standard intracellular recording techniques were used on cultured cells under an inverted microscope (Eclipse TE200, Nikon Instruments, Tokyo, Japan) as previously described (Fiumara et al. 2005; 2007). Briefly, the cells were impaled with glass intracellular electrodes, filled with 2.5 M KCl (resistance ~10 MΩ). Signals were amplified by an Axoclamp 900A amplifier (Axon Instruments, Union City, CA, USA) in current clamp mode, digitally converted by means of a Digidata 1322A analog/digital converter (Axon Instruments) and monitored, recorded and analyzed with pClamp software (Axon Instruments; RRID: rid_000085) on a personal computer. Specifically, signals were recorded with Axoscope software and recorded traces were analyzed with Clampfit software.

**Sniffer detection of neurotransmitter release**

The evaluation of neurotransmitter (NT) release from single C1 neurons was done by using a freshly isolated 5-HT-sensitive B2 neuron from the *Helix* buccal ganglia as an assay cell (sniffer) (Ghirardi et al., 2001; Fiumara et al., 2001). We took particular care in the micromanipulation of the impaled sniffer cells above the neurite outgrowth spreading from the C1 neurons. The membrane potential of the B2 sniffer neuron was kept at -80 mV. The C1 neurons were intracellularly stimulated with depolarizing current pulses to fire a train of action potentials (10 Hz for 5 or 40 sec). The sniffer responds to the 5-HT released from the varicosities in the vicinity and the amount of 5-HT released from the stimulated C1 neuron was estimated as the amplitude of the depolarization recorded from the sniffer neuron.

**Assessment of synaptic connectivity and plasticity**

Connectivity and activity dependent plasticity were analyzed as previous described (Fiumara et al., 2005). The presence and the type (electrical vs. chemical) of synaptic connections between the paired C1 and B2 neurons were assessed injecting hyperpolarizing or depolarizing currents into C1 neurons and analyzing the effect on the membrane potential of B2. Pairs were considered to be electrically coupled when the presynaptic injection of

hyperpolarizing current (0.5 nA for 2 sec) caused detectable hyperpolarization in the follower cell (see Fig. 6B). The coupling rate was calculated as the ratio between postsynaptic and presynaptic membrane hyperpolarization amplitude. Pairs were considered to be chemically coupled when presynaptic action potentials (AP) evoked excitatory postsynaptic potentials (EPSPs) with a short delay (at least 5 msec) after the peak of the presynaptic AP (Fig. 6B, dashed lines). In electrical–chemical mixed synapses, both transmissions occurred simultaneously and presynaptic APs determined a two-phase postsynaptic response. Here, the two components can be easily distinguished by the synaptic delay and the relatively slow rise kinetic of the chemical C1–B2 connection (Fig. 6B).

To investigate the activity-dependent plasticity, we used only chemical connected couples. Stimulations were delivered by intracellular injection of suprathreshold depolarizing current pulses (30 msec each), triggered by a S88 Dual Output Stimulator (Grass technologies, Warwick, RI, USA). During stimulation protocols the basal membrane potential of the postsynaptic B2 neuron was kept hyperpolarized to -80 mV to prevent firing. Paired-pulse facilitation (PPF) was estimated as the ratio between two EPSPs evoked by two presynaptic APs with a 500 msec interspike-interval (ISI). Frequency facilitation (FF) was evoked with 5 pulses at 2 Hz and it was estimated as the ratio of the 5$^{th}$ EPSP with respect to the 1$^{st}$ one. To induce post-tetanic potentiation (PTP), the presynaptic neuron was stimulated to fire at a basal rate of 0.05 Hz (basal stimulation), after 5 APs a 2 sec tetanic stimulation (10 Hz) was applied, and 0.05 Hz stimulation was resumed 30 sec after the end of the train. For statistical comparisons, the amplitude of the post-train EPSPs was normalized to the mean amplitude of the five pre-train EPSPs.

**Estimation of the $RRP_{syn}$ size**

The size of the RRP of synchronous release ($RRP_{syn}$) was calculated using the cumulative amplitude analysis (Schneggenburger et al., 1999, 2002). C1 neurons were stimulated by a

train (10 Hz for 10 sec) and the $RRP_{syn}$ was determined by summing peak EPSP amplitudes during the first 50 repetitive stimuli. During this depleting stimulus the EPSPs declined and reached a steady-state, typically interpreted as the ongoing replenishment of the depleted RRP (Schneggenburger et al., 1999). The number of data points to include in the linear fitting of the steady-state phase was evaluated by calculating the best linear fit, including the maximal number of data points starting from the last (Fig. 8D). The best linear fit was then back-extrapolated to time 0, and the interception with the y-axis was used as an estimate of the size of the $RRP_{syn}$, expressed in mV. The slope of the regression line provided an indicator of the rate of vesicle replenishment. EPSPs of the first 5 sec of tetanus were also normalized against the 1$^{st}$ EPSP of the train and plotted as a function of time in order to better appreciate the ratio of each EPSP with respect to the first one.

**Statistical analysis**

Data were expressed as mean values ± standard error of mean (s.e.m.) Statistical analysis was performed using GraphPad Prism version 5 (GraphPad Software, San Diego, CA; RRID: rid_000081). Statistical significance between two or more groups was assessed using Fisher's exact (FE)–test, two tailed Student's t-test (normal or Welch's corrected when appropriate), or ANOVA (one or two-way when appropriate) followed by the Bonferroni post-hoc test, respectively. Significance levels were set at $P < 0.05$.

## Results

### Quantification of helSyn targeting and knock-down.

Different immunocytochemical studies have demonstrated that Syn isoforms are distributed in a punctated pattern along neurites, and there are differences in the targeting properties of the various Syn isoforms, according to the specific structural domain composition. Similar to mammalian orthologous, the punctated distribution of helSyn has been observed in intact central nervous system (Ghirardi et al., 1996) and in isolated cultured cells (Ghirardi et al., 1996; Fiumara et al., 2007; Giachello et al., 2010, 2013).

As previously observed, using the serotonergic C1 neuron of *Helix* snail, immunocytochemical staining showed a punctated distribution in helSyn, predominantly localized in varicosities along neurites (Fig. 1A and B). However, in order to precisely measure helSyn protein expression levels in varicosities, the immunostaining intensity alone is not an appropriate measure, since this value is affected by the volume of the cellular compartments. For this reason, we decided to use a ratiometric imaging method called Targeting Factor (TF) (Gitler et al., 2004a). Cells were microinjected with a plasmid codifying EGFP (pNEX-EGFP), a free diffusion dye that let us visualize the volume of cellular compartments (Fig. $1B_{I,}$ green signal), and then helSyn distribution was estimated by anti-helSyn antibody immunofluorescence analysis (Fig. $1B_{II,}$ red signal). Fluorescence intensity of both signals (helSyn and EGFP) was quantified on identified varicosities and on its adjacent neurite segments and subsequently the TF was estimated (Fig. $1B_{III}$). In single C1 *Helix* neurons (n = 12), we obtained a helSyn TF of 0.32 ± 0.04, confirming its positive targeting to the varicose structures. Similar TF values have been reported for human Syn isoforms, like hSynIb (Gitler et al., 2004a).

TF was subsequently used to quantify time-dependent changes in helSyn expression level during asRNA over-expression (Fig. 1A). We found no difference in the immunostaining intensity of helSyn between the cells expressing EGFP protein (EGFP+, n = 9) and the

injected cells that do not expressed EGFP (EGFP-, n = 10) ($P > 0.05$). Conversely, when cells were co-injected with pNEX-EGFP and pNEX-helSynAS, the antisense expression correlates with a time-dependent reduction in the amount of helSyn staining ($F_{(4,36)} = 7.52$, $P = 0.0002$, One-way ANOVA), confirming significant protein loss after 48 hr (6.92% of control value, n = 9, $P < 0.01$, Bonferroni's multiple comparison post-hoc test) and 72 hr (10.67% of control value, n = 7, $P < 0.01$, Bonferroni's multiple comparison post-hoc test) following asRNA expression.

**Impairment in neurite linear outgrowth, branching and varicosity formation due to helSyn knock-down.**

Since there are conflicting reports on Syn roles in neurite outgrowth among single, double and triple knock-out mice models (Ferreira et al., 1994, 1995, 1998, 2000; Gitler et al., 2004b; Cesca et al., 2010; Valtorta et al., 2011), we analyzed the effects of *Helix* Syn knock-down on neurite linear outgrowth and branching. In order to analyze linear outgrowth we used two starting conditions. In the first case (Fig. 2A-C), cells were isolated and plated with the initial segment of their original axons. After attachment, cells were microinjected with the plasmids, and neurite growth was determined every 24 hr and normalized against the growth of control cells at the moment that asRNA expression was visually confirmed ($T_0$ as 100%). helSynKD cells (n = 7) showed a significant slowdown in neurite outgrowth after asRNA expression was confirmed, with respect to the control cells (n = 6) (treatment $F_{(1,46)} = 53.36$, $P < 0.0001$, time $F_{(4,46)} = 81.70$, $P < 0.0001$ and interaction $F_{(4,46)} = 7.74$, $P = 0.0001$, two-way ANOVA). 24 hr after the beginning of asRNA expression, the neurites appeared 33.1 % shorter compared to control cells ($P < 0.01$, Bonferroni's *post hoc* test), 43.0% shorter at 48 hr ($P < 0.001$, Bonferroni's *post hoc* test) and 47.5% shorter at 72 hr ($P < 0.001$, Bonferroni's *post hoc* test).

In the second condition, in order to better appreciate the effect of Syn silencing, we used cells in soma-configuration (Fiumara et al., 2005), cells were microinjected, kept in suspension and plated 24 hr after the starting of asRNA expression (Fig. 2D-F). In this configuration, the decrease in neurite linear outgrowth of Syn-silenced cells (n = 13) compared to controls (n = 12) was more pronounced (treatment $F_{(1,78)} = 250.4$, $P < 0.0001$, time $F_{(3,78)} = 112.9$, $P < 0.0001$ and interaction $F_{(3,78)} = 37.79$, $P < 0.0001$, two-way ANOVA). helSynKD cells showed reductions in the neurite outgrowth of 80.3% at 24 hr ($P < 0.001$, Bonferroni's *post hoc* test), 76.7% at 48 hr ($P < 0.001$, Bonferroni's *post hoc* test) and 70.6% at 72 hr ($P < 0.001$, Bonferroni's *post hoc* test) compared to control cells.

Furthermore, the knocking down of helSyn had a profound effect on the branching of newly sprouting neurites. Since 48 hr after plating, the neuritic field of the helSynKD cells (n = 13) showed a strong reduction with respect to control cells (n = 8) (treatment $F_{(1,190)} = 32.90$, $P < 0.0001$, distance $F_{(10,190)} = 18.24$, $P < 0.0001$ and interaction $F_{(10,190)} = 11.84$, $P < 0.0001$, two-way ANOVA) (Fig. 3).

In addition, down regulation of helSyn reveals a marked decrease in the total number of varicosities with respect to control cells. When cells were plated with the initial segment of their original axons there was a -40.70% decrease in the number of varicosities, with respect to control cells (100.00 ± 6.15 %, n = 7 in control cells; vs. 59.30 ± 5.60 %, n = 10 in helSynKD cells) ($t_{(15)} = 4.82$, $P < 0.001$). In soma-configuration, we observed a stronger impairment in the formation of varicosities, with an -84.64% decrease in helSynKD cells (n = 14) with respect to control cells (n = 10) ($t_{(22)} = 5.46$, $P < 0.0001$) (Fig. 4A). The area of the varicosities generated was also measured, finding varicosities 38.96% smaller in helSynKD cells (n = 9) with respect to control cells (n = 10) ($t_{(17)} = 3.74$, $P = 0.0016$) in soma-configuration (Fig. 4B). A small decrease (-10.49%) was also observed when cells were

plated with their axon, however in this condition the difference was not statistically significant (P = 0.18, t-test).

**helSyn silencing evoked increased neurotransmitter release from single C1 somata during short tetanic stimulations.**

Serotonin release from isolated C1 neurons was detected by using B2 neurons, one of its physiological targets. Freshly dissociated B2 neurons (sniffer) were micromanipulated in contact with the neuritic arbor of the C1 neurons. Neurotransmitter release was evoked by electrical stimulation of C1 at 10 Hz for 5 or 40 sec, and measured as the amount of depolarization recorded in the B2 sniffer.

During the 5 sec stimulation (Fig. 4C), the B2 response was two times greater when helSynKD cells were stimulated (10.01 ± 2.04 mV, n = 17), compared with control cells (4.45 ± 1.00 mV, n = 11) (Welch-corrected $t_{(22)} = 2.45$, P = 0.023) (Fig. 4D), suggesting an enhanced evoked neurotransmitter release during tetanic stimulation in the helSynKD cells. The maximal amplitude of sniffer depolarization induced by 40 sec stimulation (Fig. 4E) in the helSynKD cells, as well as in control cells, was similar (13.06 ± 1.99 mV, n = 17 in helSynKD cells; vs. 12.52 ± 1.95 mV, n = 11 in control cells) (P = 0.853, t-test) (Fig. 4F).

**helSyn reduction affects the occurrence of chemical synapses, but not basal transmission.**

C1 neurons (control and helSynKD) in soma-configuration were coupled to B2 neurons (Fig. 5A) and recorded 48 hr later to allow synapse formation. We previously observed that in this configuration C1 and B2 neurons can form chemical and mixed synapses (Fig. 5B) (Fiumara et al., 2005) and the establishment of functional synapses is strongly affected by the phosphorylation state of helSyn (Giachello et al., 2010). In control cells, 81.48% of the C1-B2

pairs (n = 27) were able to generate functional synapses, 51.85% of tested pairs presented pure chemical synapses and 29.63% presented mixed synapses. On the other hand, only the 40.74% of the helSynKD cells tested (n = 27) were able to generate functional synapses with the B2 cells, 25.93% were pure chemical synapses and 14.81% were mixed synapses (Fig. 5C). In summary, in helSynKD cells synaptogenesis was decreased 50% with respect to control cells (P = 0.0047, FE test), but no significant differences were observed in the proportion of chemical and mixed connections developed by control or helSynKD cells (P = 1.00, FE test). In addition, no pure electrical synapses were observed in any of the cases.
In the mixed synapses the electrical coupling was smaller than 10% in both control (9.99 ± 2.15%, n = 8) and helSynKD cells (7.09 ± 0.84%, n = 4) (P = 0.38, t-test). Despite the reduced occurrence of chemical synapses, the mean amplitude of the basal EPSP evoked by a single presynaptic AP was statistically similar between the helSynKD and control cells (0.56 ± 0.09 mV, n = 11 in helSynKD cells; vs. 0.64 ± 0.09 mV, n = 22 in control cells) (P = 0.58, t-test) (Fig. 5D).

**helSyn knock-down effects on short-term synaptic plasticity.**

It has been shown that several *Helix* monosynaptic connections undergo different forms of short-term homosynaptic plasticity (Fiumara et al., 2005) and in some of them Syn have been involved (Cesca et al., 2010). In our model we tested paired-pulse facilitation (PPF), frequency facilitation (FF) and post-tetanic potentiation (PTP). PPF was elicited with interspike intervals of 100 and 500 msec ($PPF_{100msec}$ and $PPF_{500msec}$) and FF was evoked using short trains of five presynaptic APs at 2 Hz. The degree of facilitation was estimated as the ratio between the $5^{th}$ and the $1^{st}$ EPSP (Fiumara et al., 2005). No statistical difference was observed in the $PPF_{100ms}$ (1.23 ± 0.15, n = 10 in helSynKD cells; vs. 1.00 ± 0.11, n = 18 in control cells) (P = 0.22, t-test) (Fig 6A) or the $PPF_{500msec}$ (1.15 ± 0.09, n = 8 in helSynKD

cells; vs. 1.24 ± 0.12, n = 14 in control cells) (P = 0.60, t-test) (Fig. 6B) or FF (2.18 ± 0.63, n = 8 in helSynKD cells; vs. 2.01 ± 0.30, n = 14 in control cells) (P = 0.78, t-test) (Fig. 6C). The PTP time course after a 2 sec tetanic stimulation was similar in both control and helSynKD cells (Fig. 6D). The degree of potentiation was estimated as the percentage of increase in the EPSP evoked 30 sec after the tetanic stimulation normalized to the mean of 5 pre-train EPSPs evoked at 0.05 Hz (Fiumara et al., 2005). We observed high variability, but no statistical differences between helSynKD (291.3 ± 74.7%, n = 9) and control cells (253.8 ± 43.5%, n = 16) ($t_{(23)} = 0.47$, P = 0.64) (Fig. 6D).

**Faster neurotransmitter release in monosynaptic circuits**

We have shown that there are no significant differences in the basal EPSPs evoked in targets of control and helSynKD cells (Fig. 5D), although a stronger neurotransmitter release is elicited by a high frequency stimulation in Syn-silenced isolated C1 neurons (Fig. 4C). Therefore, we tested the effect of high frequency stimulation (a 10 Hz train of APs by 10 sec) on neurotransmitter release from C1 neurons chemically coupled to B2 neurons (Fig. 7A). The depolarization of the postsynaptic B2 neuron was measured at half and at the end of the train. In the first 5 sec of stimulation (half of the stimulation) the cells depleted of Syn evoked a stronger B2 depolarization (17.80 ± 2.43 mV, n = 11), than control cells (11.83 ± 1.60 mV, n = 19) ($t_{(28)} = 2.14$, P = 0.042) (Fig. 7B). Towards the end of the 10 sec stimulation there is no statistical difference in the depolarization evoked in B2 contacting either helSynKD (12.17 ± 1.82 mV, n = 11) or control cells (12.10 ± 1.46 mV, n = 19) (P = 0.98, t-test) (Fig. 7C). During the first 5 sec of stimulation the helSynKD cells presented a stronger facilitation than control cells, as showed by the normalized EPSPs (Fig. 7D). These data agree with the neurotransmitter release estimated for the isolated C1 neurons by using sniffer B2 cells. In addition, we observed a marked run-down of the evoked EPSPs towards the end of the tetanic

stimulation in the C1-B2 pairs where Syn was silenced (Fig 7A). This might suggest a different handling of the vesicle pools.

In order to estimate the total size of the $RRP_{syn}$ and the rate of vesicle replenishment a rapid depletion protocol was used (Schneggenburger et al., 1999), protocol previously used in *Helix* neurons (Giachello et al., 2013). Both cumulative profiles presented a rapid rise followed by a slower linear increase (Fig. 7E). Since it has been demonstrated that the slow linear rise corresponds to the equilibrium between the depletion of the RRP and their replenishment, the back-extrapolation of a fitted line to time 0 yields a rough estimation of the size of the RRP of synchronous release ($RRP_{syn}$). Syn knock-down was associated with an increase in the mean size of the $RRP_{syn}$ from 5.81 ± 1.58 mV (n = 9) in control cells to 13.15 ± 3.16 mV (n = 8) in helSynKD cells ($t_{(15)} = 2.15$, P = 0.048) (Fig. 7F). No changes in the replenishment rate of the RRP was observed, since there is no statistically significant difference in the slope of the fitted lines (P = 0.83, t-test) (Fig. 7G).

## Discussion

Since Syn roles in synapses genesis and functioning is still unclear and different mice models showed sometimes conflicting results, in the present study we described the effects of Syn knock-down on a monosynaptic connection *in vitro*, reproducing a known physiological synapse.

As previously observed (Ghirardi et al., 1996; Fiumara et al., 2007; Giachello et al., 2010) helSyn presented a positive targeting to varicosities, and we showed that its TF was slightly higher than that observed in human Syn Ib (Gitler et al., 2004a). Constitutive expression of an asRNA allowed for the long term inhibition of helSyn synthesis, and protein levels decreased in a time-dependent manner, as a function of the protein half-life, reaching up to 90% inhibition after 48-72 hr. Neurite outgrowth correlated with helSyn inhibition, and suppression of helSyn before plating resulted in a stronger negative effect on neurite elongation and branching. The role of Syn on neurite outgrowth is still unclear, mainly because experimental results are controversial. SynI-deficient mammalian neurons showed neurites that elongated at a slower rate and were less branched than WT (Chin et al., 1995; Ferreira et al., 1998). SynII-deficient neurons were unable to elongate their processes or they developed short undifferentiated neurites (Ferreira et al., 1994, 1998). Moreover, neurons lacking SynIII failed to elongate axons (Ferreira et al., 2000). However, double and triple Syn KO models showed an absence of the deleterious effects of each individual deletion, and neurite development was largely restored (Ferreira et al., 1998; Valtorta et al., 2011). The likely explanation is the occurrence of compensatory mechanisms developed when two or three Syn genes are deleted (Rosahl et al., 1995). We cannot exclude the presence of compensatory mechanisms in helSynKD cells when we suppressed Syn synthesis with the asRNA; however, the robust decrease in neurite elongation and branching supports the important role of Syn on neurite development.

We also showed a remarkable decrease in number and size of presynaptic varicosities in helSynKD cells, and the number of functional connections developed between pairs of C1-B2 neurons was decreased 50 % on these cells. These data agree with previous reports where the manipulation of Syn phospho-levels decreased the formation of functional connections between *Helix* neurons (Giachello et al., 2010), and supports the proposed role of Syns in the formation and stabilization of synapses (Cesca et al., 2010).

We observed a -40% decrease in the total number of varicosities when the helSynKD cells were plated with their original axon, and a stronger decrease (-84%) when cells were plated in soma-configuration which represent an extreme condition for cell outgrowth. These results could be consistent with the -70% decrease in synapse formation quantified using synaptophysin immunoreactive spots after SynII suppression with asRNA (Ferreira et al., 1995) or the less intense decrease of -28% observed in glutamatergic synapses from cells treated with SynI small interference RNA (siRNA) (Perlini et al., 2011), and highlights the important role of Syn proteins in the establishment of synapses.

Actin cytoskeleton dynamics is associated with elongation and branching of neurites, generation of varicosities, and formation and stabilization of synapses (Cesca et al., 2010; Stiess and Bradke, 2011; Schmidt and Rathjen, 2010; Gallo, 2011; Giachello et al., 2012). Moreover, it is known that Syn produces actin nucleation and participates in cytoskeleton structure, interacting with spectrin, tubulin, annexin, calmodulin, lipids and neurofilaments (Cesca et al., 2010). Therefore, it is possible that Syn inhibition creates cytoskeleton alterations associated with aberrant growth, fewer and smaller varicosities and decreased synapse stabilization.

We tested the amplitude of the EPSPs evoked by control cells and Syn-silenced cells, and no differences were observed. EPSPs are determined by variables like the number of releasing sites (N), and the probability of vesicle release ($P_r$) (Schneggenburger et al., 2002). In

helSynKD cells we observed a reduction in varicosity number, which may indicate a smaller N, without detectable changes in the basal EPSP amplitude. This apparent discordance could be associated to an increased $P_r$ in helSynKD cells. Several authors have proposed that $P_r$ is dependent on a balance between two processes: the probability of release, which is dependent on calcium currents, and the size of the RRP (Saviane et al., 2002), expressed as: $P_r = P_r(Ca^{2+})$ x $P_r$(Ves).

The interplay between these processes at the moment of arrival of each spike would determine the EPSP amplitude and the presence of facilitation or depression (Saviane et al., 2002). Our results point to an increased $RRP_{syn}$ in helSynKD cells with respect to control cells, possibly reflecting an increased vesicle availability [↑$P_r$(Ves)] and subsequent increase in $P_r$, which could compensate for the decrease in N, evoking similar single EPSPs as observed in control cells. In order to better characterize these results we are also currently studying the possible changes in $Ca^{2+}$ currents and quantal size.

In addition to the increased RRP, we also observed a decreased capacity of maintaining NT release for long periods of high frequency activity (10 sec at 10 Hz). According to these results we can infer the likely events occurring during tetanic stimulation (Fig. 9). In control cells, a single AP evoked the release of a small fraction of the RRP (Reyes et al., 1998; Schneggenburger et al., 1999), leading to a mean EPSP of 0.64 mV from an estimated $RRP_{syn}$ of 5.81 mV. At high frequency stimulation, the continuous spiking activity increases the residual $Ca^{2+}$ [↑$P_r(Ca^{2+})$], thus promoting the release of more vesicles from the RRP, until depletion. Afterwards, the control cells are able to keep depolarized their postsynaptic targets (Fig. 7A, black record, and 8A).

Conversely, in helSynKD cells the increased NT release at the beginning of the stimulation and subsequent run-down in the postsynaptic response suggest an impairment in the handling of the vesicle pools (Fig. 7A, gray record). When Syn is silenced (Fig. 8B) it is possible that

SV from the RP gained a higher mobility (Orenbuch et al., 2012), compromising RP size and increasing RRP (estimated $RRP_{syn}$ = 13.15 mV). An increased $P_r$(Ves) could allow a basal EPSP amplitude (0.56 mV) comparable to that of control cells. During high frequency stimulation, the increased RRP and $P_r$(Ves) induce the release of an increased number of vesicles, evoking a stronger B2 response, until the RRP depletion (Fig. 7A). Subsequently, a compromised RP could be related to synaptic fatigue and run-down in the postsynaptic response in the second half of the 10 sec tetanus.

Our model is consistent with literature on TKO mice models where a similar excitatory postsynaptic current amplitude (Gitler et al., 2004b), increased RRP (Kile, 2010; Farisello et al., 2013), decreased RP (Gitler et al., 2004b; Orenbuch et al., 2012) and increased SV mobility (Orenbuch et al., 2012) with respect to WT mice has been reported. In addition, the decreased RP is one of the features observed in most single, double and triple KO models (except for SynIII KO) (Cesca et al., 2010).

Several authors have observed a decreased total number of SV in excitatory synapses of TKO mice (Gitler et al., 2004b; Siksou et al., 2007; Cesca et al., 2010; Orenbuch et al., 2012), but this apparently discordant data could be explained by the increased vesicle mobility, which can induce movement of SV outside of the presynaptic terminal, decreasing the total number of SV observed in this structure by electron microscopy, but probably increasing the pool of vesicles localized in the axons (axonal pool) (Denker and Rizzoli, 2010; Orenbuch et al., 2012). These SVs could be released during high frequency stimulation only if the accumulation of residual $Ca^{2+}$ is strong enough for their recruitment, increasing Pr($Ca^{2+}$).

Taken together these data strongly support the role of Syn in the establishment of the vesicle pools and their role in the maintenance of neuron capacity to maintain SV exocytosis under high frequency stimulation, regulating the constant resupply of SVs.

Concerning the role of Syn in short-term synaptic plasticity, we observed no significant differences on paired-pulse facilitation with different ISIs, or frequency facilitation. Similar results were reported by Fiumara et al. (2007) where the over-expression of either helSyn WT or a non-phosphorylatable mutant does not affect frequency facilitation. In literature, there is evidence that Syn is implicated in PTP both from mammal (Farisello et al., 2013) and invertebrate models (Humeau et al., 2001). In *Helix* we previously reported that preventing helSyn phosphorylation is sufficient to impair PTP (Fiumara et al., 2007; Giachello et al., 2010). Here, we have found no statistical differences in the degree of potentiation in helSynKD cells although the same induction protocol was applied (2 sec at 10 Hz, as described in Fiumara et al., 2007). One possibility is that the presynaptic overexpression of a non-phosphorylatable Syn mutant may act in a dominant-negative manner by affecting vesicle clustering and severely impairing PTP. This may suggest that the interconversion cycle of dephosphorylated-phosphorylated Syn rather than protein abundance is more relevant for PTP expression. Another possibility that we cannot exclude is that the mechanism underneath PTP induction is different in control cells and Syn-silenced cells. We have previously showed that inhibitors of CaMK and PKA impair PTP in C1-B2 synapsis (Fiumara et al., 2007) and future studies will be needed in order to test if PTP induction in helSynKD cells is similarly affected by these inhibitors.

It has also been suggested that PTP impairment could be associated with a depletion of the RP and RRP exhaustion during the conditioning stimulus, which cannot be replenished when the PTP was tested (Humeau et al., 2001). Another possibility could be the incomplete RRP depletion during the 2 sec conditioning stimulus or a faster RRP replenishment between the tetanus and the resumed basal stimulation.

In summary, we used a simple monosynaptic model in which Syn protein was knocked down in the presynaptic terminals, and the results of our experiments highlight the important role of

Syns in the development of neurites and in the formation of varicosities. This study shows that the development of functional synapses is not dependent solely on Syn phosphorylation status as previously indicated, but it is also dependent on the correct expression of Syn proteins. Our results underscore the importance of Syn in the assembly and maintenance of synaptic vesicle pools, thus affecting the RRP size and the capacity of the cell to respond to high frequency stimulation by tuning synaptic vesicle availability.

**Acknowledgment**

We thank Virginia Eterno and Andrea Cerase for their technical support. We would also like to thank Ferdinando Fiumara for the technical support, manuscript correction and helpful comments, Adarli Romero for helpful comments and Paul Hanson for language correction.

**Conflict of Interest Statement**

Authors disclosed any actual or potential conflict of interest including any financial, personal or other relationships with other people or organizations influencing the present article.

**Role of authors**

The experiments included in this study were performed and the manuscript was mainly written by OB. CNGG participated in experiment planning, analysis and valuable discussion. PGM and MG participated in experiment planning and discussion. All authors participated in manuscript correction.

**References**

Cesca F, Baldelli P, Valtorta F, Benfenati F. 2010. The Synapsins: key actors of synapse function and plasticity. Prog Neurobiol 91:313-348.

Chiappalone M, Casagrande S, Tedesco M, Valtorta F, Baldelli P, Martinoia S, Benfenati F. 2009. Opposite changes in glutamatergic and GABAergic transmission underlie the diffuse hyperexcitability of synapsin I-deficient cortical networks. Cereb Cortex 19:1422-1439.

Chin LS, Li L, Ferreira A, Kosik KS, Greengard P. 1995. Impairment of axonal development and of synaptogenesis in hippocampal neurons of synapsin I-deficient mice. Proc Natl Acad Sci 92:9230-9234.

Corradi A, Fadda M, Piton A, Patry L, Marte A, Rossi P, Cadieux-Dion M, Gauthier J, Lapointe L, Mottron L, Valtorta F, Rouleau GA, Fassio A, Benfenati F, Cossette P. 2014. SYN2 is an autism predisposing gene: loss-of-function mutations alter synaptic vesicle cycling and axon outgrowth. Hum Mol Genet 23(1):90-103.

Denker A, Rizzoli SO. 2010. Synaptic vesicles pools: an update. Front Synaptic Neurosci 2:135. doi: 10.3389/fnsyn.2010.00135

Farisello P, Boido D, Nieus T, Medrihan L, Cesca F, Valtorta F, Baldelli P, Benfenati F. 2013. Synaptic and extrasynaptic origin of the excitation/inhibition imbalance in the hippocampus of synapsin I/II/III knockout mice. Cereb Cortex 23(3):581-593.

Fassio A, Patry L, Congia S, Onofri F, Piton A, Gauthier J, Pozzi D, Messa M, Defranchi E, Fadda M, Corradi A, Baldelli P, Lapointe L, St-Onge J, Meloche C, Mottron L, Valtorta F, Nguyen DK, Rouleau GA, Benfenati F, Cossette P. 2011. SYN1 loss-of-function mutations in autism and partial epilepsy cause impaired synaptic function. Hum Mol Genet 20(12):2297-2307.

Feng J, Chi P, Blanpied TA, Xu Y, Magarinos AM, Ferreira A, Takahashi RH, Kao HT, McEwen BS, Ryan TA, Augustine GJ, Greengard P. 2002. Regulation of neurotransmitter release by synapsin III. J Neurosci 22(11):4372-4380.

Ferreira A, Kosik KS, Greengard P, Han HQ. 1994. Aberrant neurites and synaptic vesicle protein deficiency in synapsin Il-depleted neurons. Science 264:977-979.

Ferreira A, Han HQ, Greengard P, Kosik KS. 1995. Suppression of synapsin II inhibits the formation and maintenance of synapses in hippocampal culture. Neurobiol 92:9225-9229.

Ferreira A, Chin LS, Li L, Lanier LM, Kosik KS, Greengard P. 1998. Distinct roles of synapsin I and synapsin II during neuronal development. Mol Med 4:22-28.

Ferreira A, Kao HT, Feng J, Rapoport M, Greengard P. 2000. Synapsin III: developmental expression, subcellular localization, and role in axon formation. J Neurosci 20(10):3736-3744.

Fiumara F, Onofri F, Benfenati F, Montarolo PG, Ghirardi M. 2001. Intracellular injection of synapsin I induces neurotransmitter release in C1 neurons of *Helix pomatia* contacting a wrong target. Neurosci 104(1):271-280.

Fiumara F, Giovedì S, Menegon A, Milanese C, Merlo D, Montarolo PG, Valtorta F, Benfenati F, Ghirardi M. 2004. Phosphorylation by cAMP-dependent protein kinase is essential for synapsin-induced enhancement of neurotransmitter release in invertebrate neurons. J Cell Sci 117:5145-5154.

Fiumara F, Leitinger G, Milanese C, Montarolo PG, Ghirardi M. 2005. In vitro formation and activity-dependent plasticity of synapses between *Helix* neurons involved in the neural control of feeding and withdrawal behaviors. Neurosci 134:1133-1151.

Fiumara F, Milanese C, Corradi A, Giovedi S., Leitinger G., Menegon A., Montarolo PG, Benfenati F, Ghirardi M. 2007. Phosphorylation of synapsin domain A is required for post-tetanic potentiation. J Cell Sci 120:3228-3237.

Gaffield MA, Betz WJ. 2007. Synaptic vesicles mobility in mouse motor nerve terminals with and without synapsin. J Neurosci 27(50):13691-13700.

Gallo G. 2011. The cytoskeletal and signaling mechanisms of axon collateral branching. Dev Neurobiol 71:201-220.

Garcia CC, Blair HJ, Seager M, Coulthard A, Tennant S, Buddles M, Curtis A, Goodship JA. 2004. Identification of a mutation in synapsin I, a synaptic vesicle protein, in a family with epilepsy. J Med Genet 41:183-186.

Ghirardi M, Casadio A, Santarelli L, Montarolo PG. 1996. *Aplysia* hemolymph promotes neurite outgrowth and synaptogenesis of identified *Helix* neurons in cell culture. Invert Neurosci 2:41-49.

Ghirardi M, Naretto G, Fiumara F, Vitiello F, Montarolo PG. 2001. Target-dependent modulation of neurotransmitter release in cultured *Helix* neurons involves adhesion molecules. J Neurosci Research 65:111-120.

Giachello CNG, Fiumara F, Giacomini C, Corradi A, Milanese C, Ghirardi M, Benfenati F, Montarolo PG. 2010. MAPK/Erk-dependent phosphorylation of synapsin mediates formation of functional synapses and short-term homosynaptic plasticity. J Cell Sci 123:881-893.

Giachello CNG, Montarolo PG, Ghirardi M. 2012. Synaptic functions of invertebrate varicosities: what molecular mechanisms lie beneath. Neural Plast 2012:670821.

Giachello CNG, Premoselli F, Montarolo PG, Ghirardi M. 2013. Pentylenetetrazol-induced epileptiform activity affects basal synaptic transmission and short-term plasticity in monosynaptic connections. PLOSone 8(2):e56968.

Gitler D, Xu Y, Kao HT, Lin D, Lim S, Feng J, Greegard P, Augustine G. 2004a. Molecular determinants of synapsin targeting to presynaptic terminals. J Neurosci 24(14):3711-3720.

Gitler D, Takagishi Y, Feng J, Ren Y, Rodriguez RM, Wetsel WC, Greengard P, Augustine GJ. 2004b. Different presynaptic roles of synapsins at excitatory and inhibitory synapses. J Neurosci 24:11368-11380.

Greco B, Managò F, Tucci V, Kao HT, Valtorta F, Benfenati F. 2013. Autism-related behavioral abnormalities in synapsin knockout mice. Behav Brain Res 251:65-74.

Humeau Y, Doussau F, Vitiello F, Greengard P, Benfenati F, Poulain B. 2001. Synapsin controls both reserve and releasable synaptic vesicle pools during neuronal activity and short-term plasticity in *Aplysia*. J Neurosci 21(12):4195-4206.

Kile BM, Guillot TS, Venton BJ, Wetsel WC, Augustine GJ, Wightman RM. 2010. Synapsins differentially control dopamine and serotonin release. J Neurosci 30(29):9762-9770.

Medrihan L, Cesca F, Raimondi A, Ligani G, Baldelli P, Benfenati F. 2013. Synapsin II desynchronizes neurotransmitter release at inhibitory synapses by interacting with presyaptic calcium channels. Nature commun 4:1512. doi: 10.1038/ncomms2515.

Orenbuch A, Shalev L, Marra V, Sinai I, Lavy Y, Kahn J, Burden JJ, Staras K, Gitler D. 2012. Synapsin selectively controls the mobility of resting pool vesicles at hippocampal terminals. J Neurosci 32(12):3969-3980.

Perlini LE, Botti F, Fornasiero EF, Giannandrea M, Bonanomi D, Amendola M, Naldini L, Benfenati F, Valtorta F. 2011. Effects of phosphorylation and neuronal activity on the control of synapse formation by synapsin I. J Cell Sci 124:3643-3653.

Reyes A, Lujan R, Rozov A, Burnashev N, Somogyi P, Sakman B. 1998. Target-cell-specific facilitation and depression in neocortical circuits. Nat Neurosci 1(4):279-285.

Rosahl TW, Spillane D, Missler M, Herz J, Selig DK, Wolff JR, Hammer RE, Malenka RC, Sudhof TC. 1995. Essential functions of synapsin-I and synapsin-II in synaptic vesicle regulation. Nature 375:488-493.

Saviane C, Savtchenko LP, Raffaelli G, Voronin LL, Cherubini E. 2002. Frequency-dependent shift from paired-pulse facilitation to paired-pulse depression at unitary CA3-CA3 synapses in the rat hippocampus. J Physiol 544(2):469-476.

Schmidt H, Rathjen FG. 2010. Signalling mechanisms regulating axonal branching *in vivo*. Bioassays 32:977-985.

Schneggenburger R, Meyer AC, Neher E. 1999. Released fraction and total size of a pool of immediately available transmitter quanta at a calyx synapse. Neuron 23:399-409.

Schneggenburger R, Sakaba T, Neher E. 2002. Vesicle pools and short-term synaptic depression: lessons from a large synapse. Trends Neurosci 25(4):206-212.

Siksou L, Rostaing P, Lechaire JP, Boudier T, Ohtsuka T, Fejtová A, Kao HT, Greengard P, Gundelfinger ED, Triller A, Marty S. 2007. Three-dimensional architecture of presynaptic terminal cytomatrix. J Neurosci 27(26):6868-6877.

Stiess M, Bradke F. 2011. Neuronal polarization: The cytoskeleton leads the way. Dev Neurobiol 71:430-444.

Valtorta F, Pozzi D, Benfenati F, Fornasiero EF. 2011. The synapsins: Multitask modulators of neuronal development. Semin Cell & Dev Biol 22:378-386.

Washbourne P, Dityatev A, Scheiffele P, Biederer T, Weiner JA, Christopherson KS, El-Husseini A. 2004. Cell adhesion molecules in synapse formation. J Neurosci 24(42):9244-9249.

**Figure legends**

**Fig.1. *Helix* Syn knock-down by asRNA constitutive over-expression.** A: Fluorescence micrographs of control and Syn-silenced cells (helSynKD) immunolabeled with a custom antibody against helSyn after 48 hr of expression. Scale bar: 5 μm. B: Quantification of helSyn by the fluorescence radiometric imaging analysis called Targeting Factor, fluorescence intensity of EGFP (I) and helSyn immunostaining (II) were quantified for each varicosity and its proximal neurites, then TF was calculated for each varicosity (III). Scale bar: 10 μm. C: helSyn protein expression was quantified using the Targeting Factor in cells expressing the asRNA for different time periods and in control cells expressing or not EGFP protein (EGFP+ and EGFP-, respectively). Each bar indicates the mean ± s.e.m. **P < 0.01.

**Fig.2. Neurite outgrowth impairment after helSyn knock-down**. Neurite outgrowth was analyzed in C1 neurons plated with the initial segment of their axons (A-C) and in C1 neurons plated as axon-reabsorbed somata (soma-configuration) (D-F). In C, control cells (●) and Syn-silenced cells (helSynKD) (○) were normalized to the control mean value measured at the moment that plasmid expression was visually confirmed ($T_0$). In F, cells were plated 24 hr after plasmid expression started and neurite outgrowth was normalized to the control mean value measured at 24 hr of plating. Scale bars: 100 μm. Each time-point represents the mean ± s.e.m. **P < 0.01, ***P < 0.001.

**Fig.3. Neuritic field decrease in Syn-silenced cells**. The branching of neurites was estimated counting the number of neurite intersections with concentric rings at intervals of 25 μm. Control cells (●) developed neuritic fields with longer neurites and a higher number of branches that cells where Syn was silenced (helSynKD) (○). Each time-point represents the mean ± s.e.m. **P < 0.01, ***P < 0.001

**Fig.4. Impairment in varicosities formation and increased neurotransmitter release in helSynKD cells.** Cell varicosities were counted using micrographs of the whole neurite field

of each cell in soma-configuration (10X magnification) and measured on micrographs with a 60X magnification. asRNA expressing cells (helSynKD) showed a smaller number of varicosities along neurites (A) and a smaller mean size of the newly formed varicosities (B). Neurotransmitter release induced by a train of action potentials (horizontal bars in C and E) in C1 neurons, control and helSynKD cells was estimated as the mean depolarization in a B2 sniffer cell. The 5 sec train (C-D) showed, an increased sniffer depolarization amplitude when helSynKD cells were stimulated. A 40 s train induced similar depolarization amplitudes (E-F). Values represent means ± s.e.m. *P < 0.05, **P < 0.01, ***P < 0.001.

**Fig.5. Syn knock-down decreased the capacity of synapse establishment without changing basal transmission.** A: Phase contrast (top) and fluorescence (bottom) micrographs of a C1-B2 pair cultured in soma-soma configuration. Scale bar: 100 μm. B: Sample recordings of chemical (left) and mixed (right) C1-B2 synapse. The basal membrane potential of B2 was kept at -80 mV to prevent firing. The top vertical dashed lines aligned with the peak of the presynaptic action potential show the EPSP short delay in chemical synapses and the postsynaptic corresponding peak in mixed (electrical-chemical) synapses. C: Occurrence of chemical and mixed connections between C1 and B2 neurons in control and Syn-deficient cells (helSynKD). D: Basal EPSP evoked in B2 neurons after a single presynaptic spike in control and helSynKD cells. Values represent means ± s.e.m.

**Fig.6. Syn knock-down effects on short-term synaptic plasticity.** Two presynaptic action potentials with 100 msec (A) and 500 msec (B) interspike-intervals were used to estimate paired-pulse facilitation ($PPF_{100msec}$ and $PPF_{500msec}$ respectively. C: Sample electrophysiological recordings of frequency facilitation (FF) in which C1 cell was stimulated to fire at 2 Hz and EPSP amplitude progressively increased during the train. Facilitation was estimated as the ratio between the fifth and the first EPSP. D: Time course of EPSP amplitude changes in control cells and Syn-silenced cells after a 2 sec tetanic stimulation at 10 Hz, post-

tetanic potentiation (PTP) percentage was estimated 30 sec after the tetanic stimulation. Values represent means ± s.e.m.

**Fig.7. Syn knock-down increased neurotransmitter release under high frequency stimulation changing synaptic vesicle pools constitution.** A: Sample electrophysiological recording from B2 postsynaptic cell during a tetanic stimulation (horizontal bar) in C1 control and Syn-depleted cells (helSynKD). B: B2 depolarization amplitude at half recording and C: at the end of the recording. D: Plot of the EPSPs (normalized against the first EPSP of the tetanus) during the first 5 sec of stimulation. E: Cumulative EPSP amplitude profiles. To estimate the size of RRP of synchronous release ($RRP_{syn}$) data points were fitted by linear regression from the last point and back-extrapolated to time 0 in control (●) and helSynKD (○) cells. F: Bar graph of the estimated $RRP_{syn}$ size. G: Slopes of the fitted lines as an estimation of vesicle replenishment rates. Values represent means ± s.e.m. *P < 0.05, ***P < 0.001.

**Fig.8. Vesicle release under high frequency stimulation in control and Syn knock-down cells (helSynKD).** A: In control cells, upon arrival of the first action potential (AP) the releasable fraction of the readily releasable pool (fast RRP) is released. Further stimulation results in the release of the rest of the RRP (slow). When stimulation continues, the reserve pool (RP) is recruited. B: In helSynKD cells there are a smaller number of varicosities, the RRP is increased with highly mobile vesicles and the RP is compromised. The first AP leads to the release of more synaptic vesicles than in control cells (slow and fast vesicles). Further stimulation evoked increased release of almost all the vesicles, leading to a strong run-down in the postsynaptic response if the stimulation is continuous. The lower panels indicate the neurotransmitter release against time and at the end postsynaptic recordings obtained during stimulation of controls and helSynKD cells are shown as inserts.

**Fig 1**

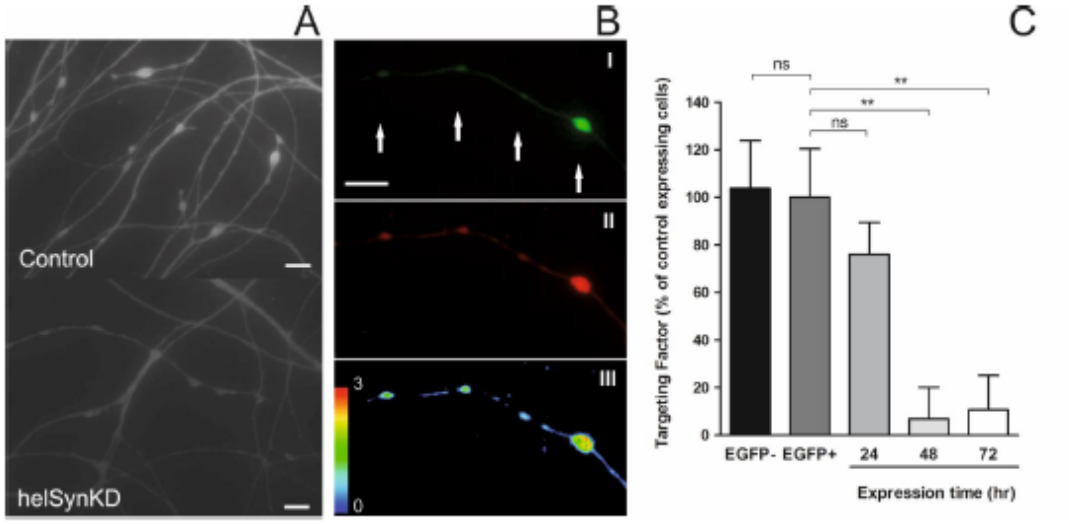


**Fig 2**

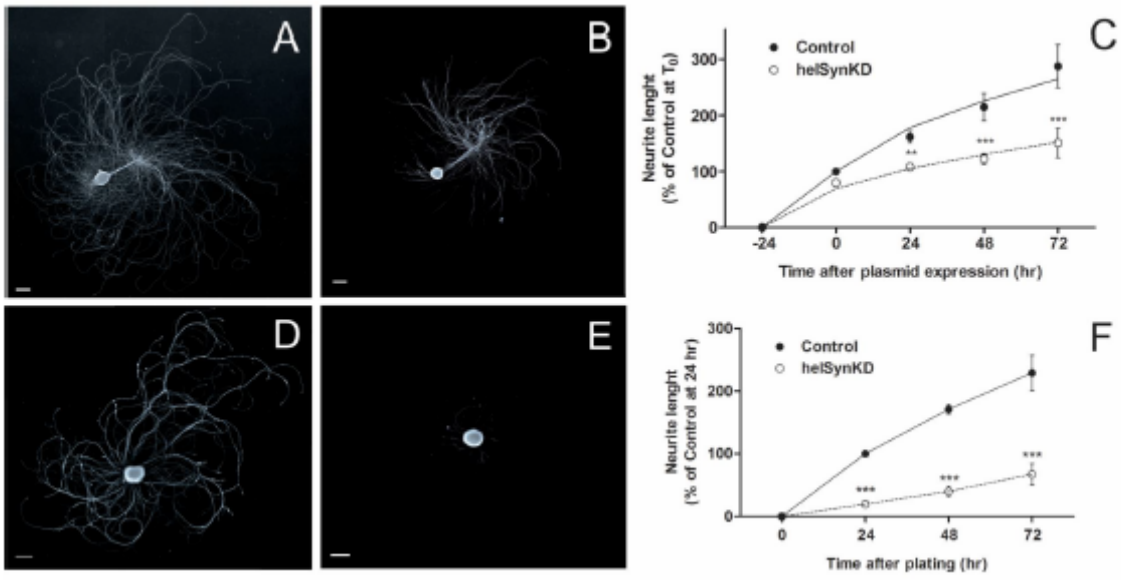


**Fig 3**

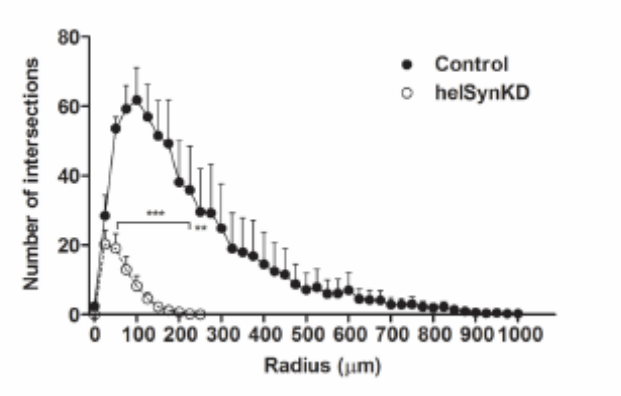
Number of intersections
Radius (μm)
Control
helSynKD
***
**

**Fig 4**

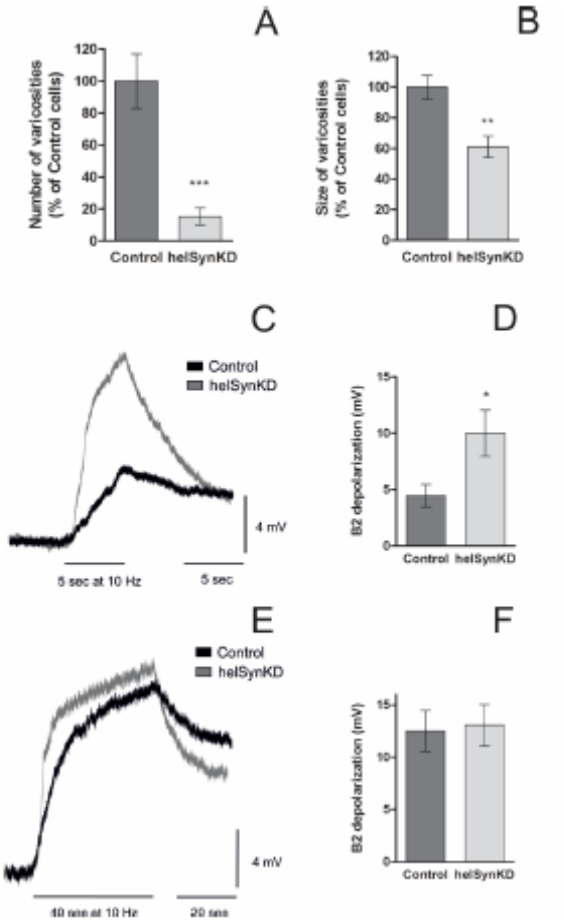
A
B
C
D
E
F
Number of varicosities (% of Control cells)
Size of varicosities (% of Control cells)
Control
helSynKD
B2 depolarization (mV)
4 mV
5 sec at 10 Hz
5 sec
40 sec at 10 Hz
20 sec

**Fig 5**

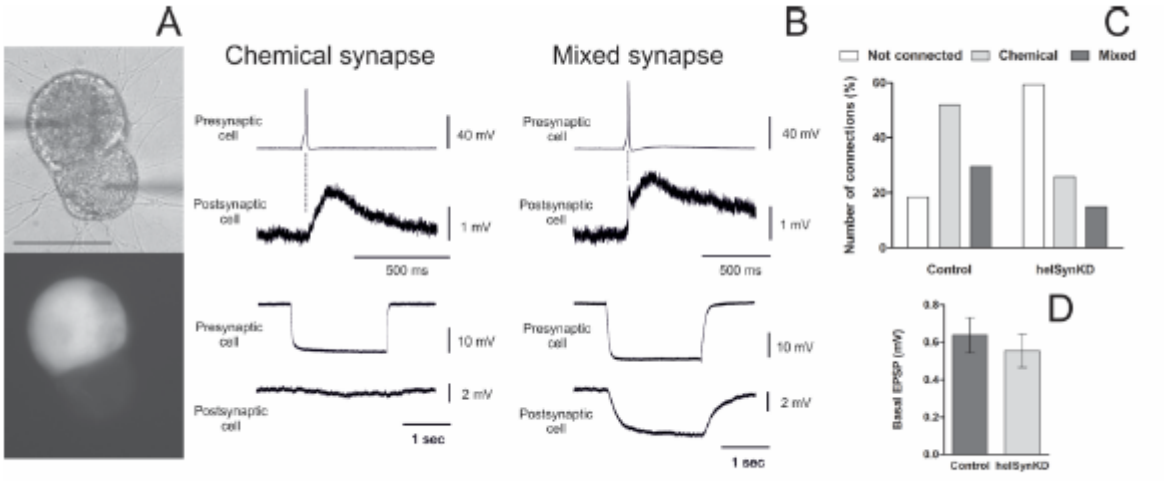
A
Chemical synapse
Mixed synapse
B
C
Not connected
Chemical
Mixed
Presynaptic cell
Postsynaptic cell
40 mV
1 mV
500 ms
10 mV
2 mV
1 sec
Number of connections (%)
Control
helSynKD
D
Basal EPSP (mV)

**Fig 6**

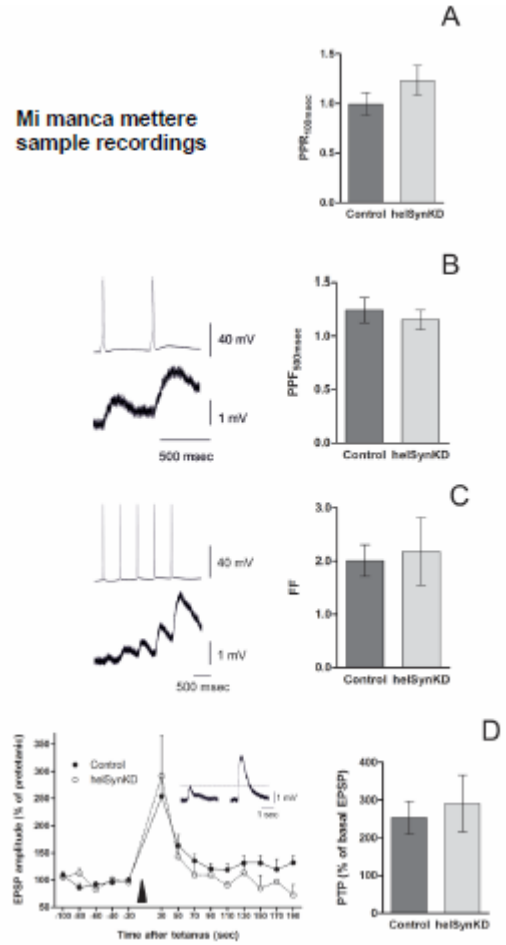
Mi manca mettere sample recordings
A
B
C
D
40 mV
1 mV
500 msec
Control
helSynKD
FF
PTP (% of basal EPSP)
Time after tetanus (sec)

**Fig 7**

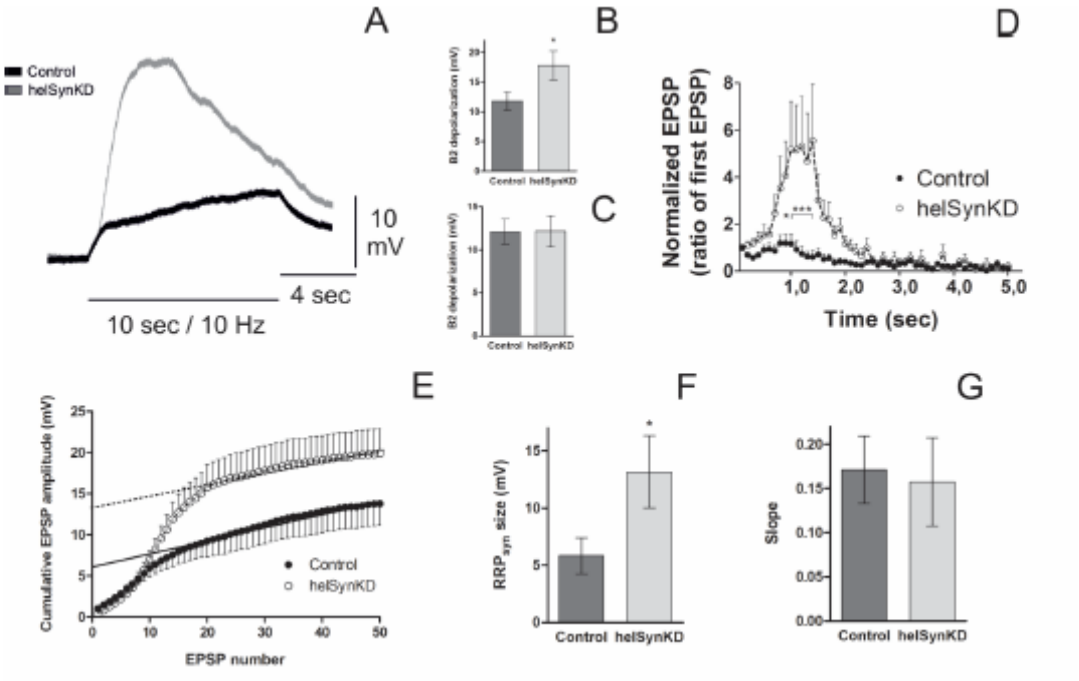
A
Control
helSynKD
10 mV
4 sec
10 sec / 10 Hz
B
B2 depolarization (mV)
Control helSynKD
C
B2 depolarization (mV)
Control helSynKD
D
Normalized EPSP (ratio of first EPSP)
Control
helSynKD
Time (sec)
E
Cumulative EPSP amplitude (mV)
Control
helSynKD
EPSP number
F
RRP sym size (mV)
Control helSynKD
G
Slope
Control helSynKD

**Fig 8**

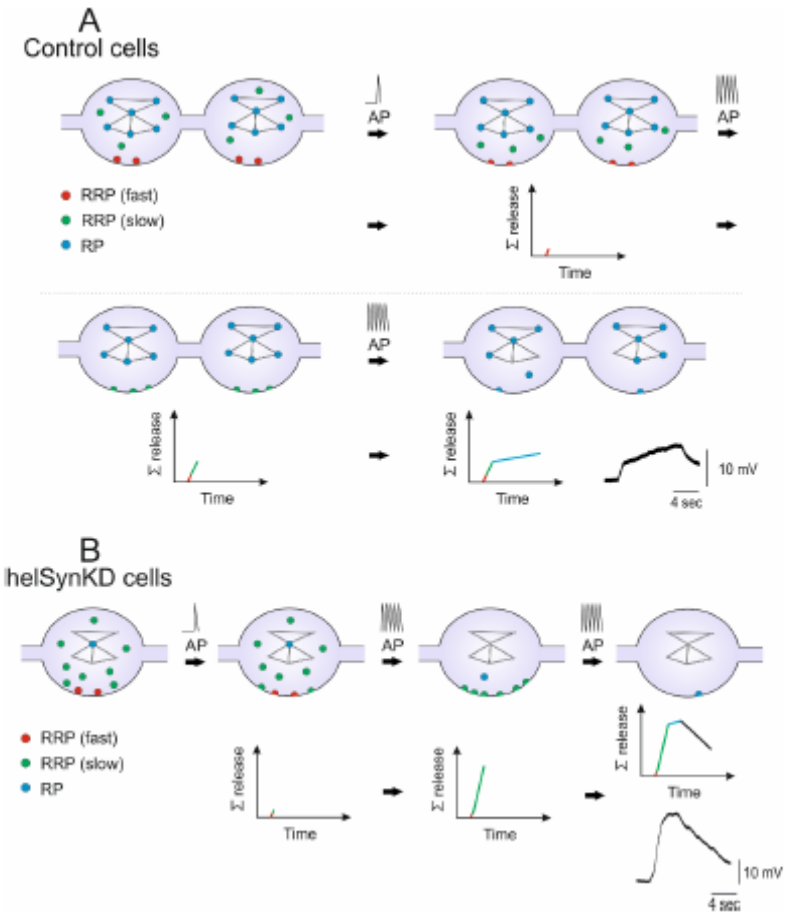
A
Control cells
AP
AP
RRP (fast)
RRP (slow)
RP
Σ release
Time
AP
Σ release
Time
Σ release
Time
10 mV
4 sec
B
helSynKD cells
AP
AP
AP
RRP (fast)
RRP (slow)
RP
Σ release
Time
Σ release
Time
Σ release
Time
10 mV
4 sec